Brittle fracture in a complex metallic compound from an atomistic viewpoint: $NbCr_2$, a case study

Frohmut Rösch and Hans-Rainer Trebin

Institut für Theoretische und Angewandte Physik, Universität Stuttgart, Pfaffenwaldring 57, 70550 Stuttgart, Germany

PACS 62.20.mj Brittleness
PACS 61.66.Fn Inorganic compounds
PACS 02.70.Ns Molecular dynamics and particle methods

Material-specific atomistic aspects of brittle fracture are studied for the first time for a complex metallic compound with realistic embedded-atom-method potentials. Crack propagation occurs on an atomic level by a successive rupture of cohesive bonds. In many theoretical models of fracture, however, a coarse-grained approach is applied and the explicit influence of the discrete nature of matter is not taken into account. In this paper, numerical experiments on the complex metallic compound $NbCr_2$ are presented to illustrate why it is necessary to perform atomistic simulations to understand details of fracture behaviour: The number, strength and orientation of bonds approached by a crack determine whether, where and how it propagates.

Introduction

In a linear elastic continuum approach, a material is assumed to follow Hooke's law. To allow the failure of a sample by perfect brittle fracture (*i.e.* without any dislocation activity), an additional criterion is needed. Following Griffith [1], crack propagation becomes possible when the so-called energy release rate G equals the surface energy of the two newly generated fracture surfaces. The linear elastic solutions for the stress field of a sharp crack experience a singularity close to the crack tip. The strength of this singularity is given by the so-called stress intensity factor K. K is a measure for the applied load and contains the geometry of the sample. Furthermore, with $G \propto K^2$, the stability of a specimen can in principle be checked. However, this picture has several drawbacks. First, the singularity shows that the derivation within linear elasticity is unphysical at the crack tip. Obviously, a linear force law is no longer valid, when atomic bonds break. Second, the discrete nature of matter is not included in a continuum picture. These problems as well as the need for an explicit fracture criterion are circumvented by the use of a direct atomistic simulation. Thomson [2] has shown that the lattice affects crack propagation. Cracks are stabilised in an *interval* around the Griffith load. This effect is called lattice-trapping. So far, the material-specific atomistic aspects of brittle fracture have been studied only in model systems (see *e.g.* [3]) or in simple configurations (see *e.g.* [4]). One extensively investigated example in the case of covalent materials is silicon [5–9]. However, in materials science and engineering, metals, intermetallics and alloys still play a central role. Although structurally complex metallic alloys often exhibit promising high temperature properties, their brittleness at low and ambient temperature limits application. So, in this study, fracture of a complex metallic alloy at low temperature is investigated. The chosen compound $NbCr_2$ forms one of the Friauf-Laves phases, which represent the largest subset of topologically close-packed intermetallic compounds [10]. With 24 atoms in the cubic unit cell, C15 $NbCr_2$ is structurally already quite complex.

Method

Dynamic fracture in $NbCr_2$ is studied by means of molecular dynamics simulations [11]. As interatomic interactions we apply embedded-atom-method potentials [12]. These were derived employing ab-initio calculations and the force-matching [13] method using VASP [14] and potfit [15, 16]. The potentials were carefully tested and validated [17, 18]. Samples consisting of about 5 million atoms are set up for the numerical experiments. A strip geometry is used to study crack

propagation with constant energy release rate for a long time. The length l of the strip is chosen to be about 0.1 μm. The dimensions of the sample are approximately $l \times \frac{l}{3} \times \frac{l}{6}$. Periodic boundary conditions are employed along the direction of the crack front. For the other directions, atoms in the outermost boundary layers are held fixed. An atomically sharp seed crack is inserted at a plane of lowest surface energy from one side to about $\frac{l}{4}$. The system then is uniaxially strained perpendicular to the crack plane up to the Griffith load ($K = K_{\mathrm{G}}$) and is relaxed to obtain the displacement field of a stable crack at zero temperature. To explore dynamic fracture without strong thermal fluctuations, a temperature of about 10^{-4} of the melting temperature is applied to the configurations with and without the relaxed crack. From the resulting configurations an averaged displacement field for this temperature is obtained. The mode I crack then is further loaded by a linear scaling of the displacement field. The response of the system is monitored using molecular dynamics techniques. The sound waves emitted by the propagating crack are damped away outside of an elliptical cylinder to prevent reflections (for details see [3, 19–21]).

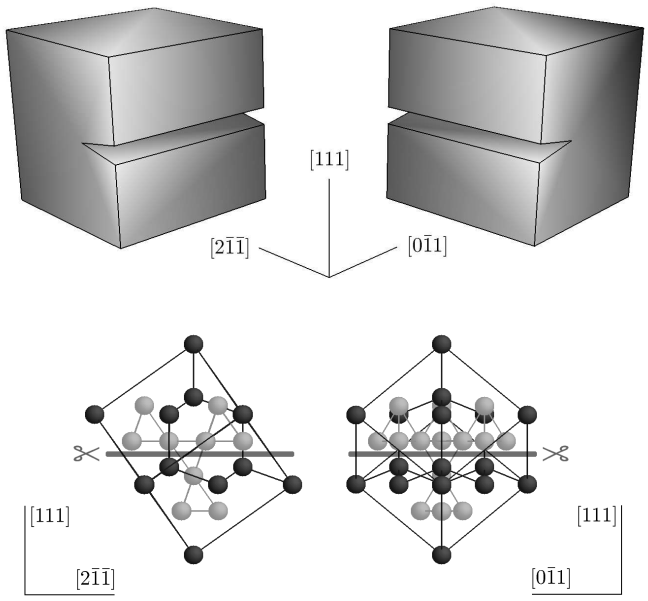

Fig. 1: Schematic drawing of the orientations of the samples. Cubic cells containing 24 basis atoms are also indicated in the corresponding arrangements. Dark (bright) balls highlight the positions of Nb (Cr) atoms. Nearest neighbours of the same kind are connected by lines. Cleavage planes are depicted by a line and a pair of scissors.

Results and discussion

To demonstrate the crucial role of lattice-trapping, we first concentrate on one aspect of the fracture simulations of the brittle compound $NbCr_2$: The dependence of fracture behaviour on the crack propagation *direction*. Two seed cracks are inserted on one and the same (111) plane of lowest surface energy. One crack is driven in [2$\bar{1}\bar{1}$] direction, the other one in [0$\bar{1}$1] direction (see fig. 1). From a simple global continuum picture, there should be no difference in fracture behaviour as the critical energy release rate would be the same for both orientations. Molecular dynamics simulations, however, give different behaviour for the two cases.

In fig. 2 sections of two geometrically scanned fracture surfaces are shown. The crack propagated from the left to the right. Due to the load of $k = K/K_{\mathrm{G}} = 1.3$, the energy in the system is already about 69% higher than needed for the generation of a flat cut. In the left part of fig. 2 the crack was driven in [2$\bar{1}\bar{1}$] direction. Apart from a few point defects due to the overload, the surface is flat. On the right hand side of fig. 2 the crack propagated in [0$\bar{1}$1] direction. The resulting surface shows higher root-mean-square and peak-to-valley roughnesses. It seems whether the crack could not decide to choose one atomic level, as the image mainly shows larger segments of two subsequent atomic layers. As a consequence, the surface energies of the two samples also differ. The surface energy is increased by 13% respectively 28% compared to the flat cut. So, the majority of the energy surplus goes into radiation.

In figs. 3 and 4 the position of the crack tip vs. time is shown for various loads. The crack speed increases with increasing load. The curves are ordered in the figures by increasing k from bottom to top. Dashed lines are linear fits to the data. The velocities are given behind the corresponding k values. At a load of $k = 1.3$ both orientations show a steady state crack propagation (third curves from the top). The velocities of the two (111) cracks differ significantly. For the nearly flat surface, the crack travels at $1.05\frac{\mathrm{km}}{\mathrm{s}}$, for the rougher surface at $0.76\frac{\mathrm{km}}{\mathrm{s}}$. The cracks propagating at constant velocity in [2$\bar{1}\bar{1}$] direction always are faster than those travelling in [0$\bar{1}$1] direction. Thus, the atomistic differences at the crack tip strongly influence a macroscopic property, the crack speed.

Despite the variation in the velocities, there are also differences in crack propagation at low loads. Fig. 3 shows that the crack starts to propagate for $k = 1.2$. For this load, an acceleration process up to about 30 ps is needed to arrive at the final velocity. The crack in fig. 4 starts moving already for $k = 1.1$. Thus, the initial barrier for crack propagation is lower than in the former case. However, after about 25 ps, the crack stops moving. For $k = 1.2$ no constant velocity can be defined. The crack arrest and the meandering motion can be understood from energy considerations. For $k = 1.1$ the energy surplus compared to the Griffith value is about 21%. As the crack propagates, the surface roughens similarly as shown in fig. 4. When the increased surface energy becomes comparable to the available energy in the system, crack propagation becomes unstable. For $k = 1.1$ this leads to crack arrest.

Thus, the numerical simulations have shown that the

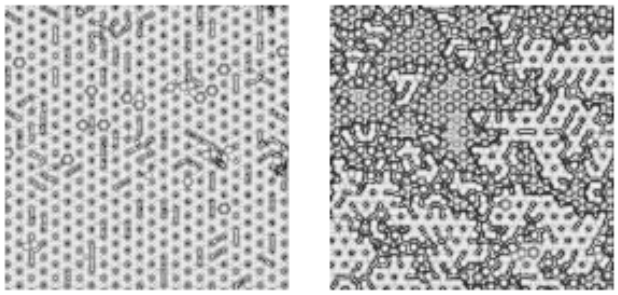

Fig. 2: 10 nm × 10 nm sections of (111) fracture surfaces geometrically scanned with a Nb atom. The crack propagated in $[2\bar{1}\bar{1}]$ (left) and in $[0\bar{1}1]$ (right) direction at the same load.

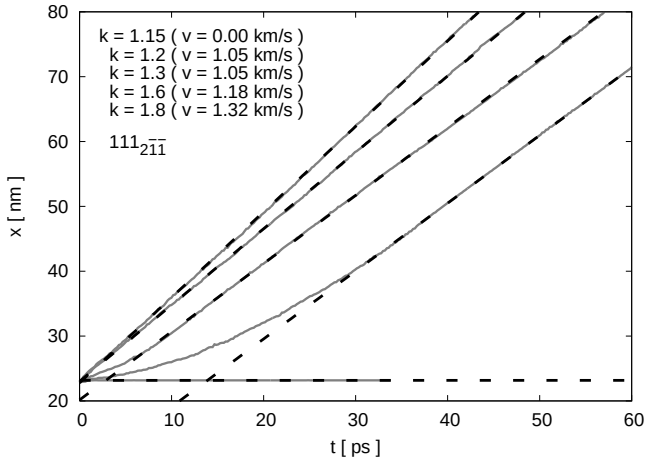

Fig. 3: Crack-tip position vs. time for a (111) crack propagating in $[2\bar{1}\bar{1}]$ direction.

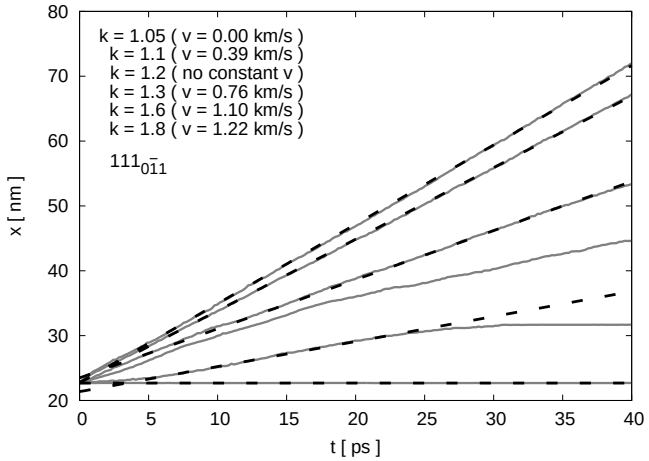

Fig. 4: Crack-tip position vs. time for a (111) crack propagating in $[0\bar{1}1]$ direction.

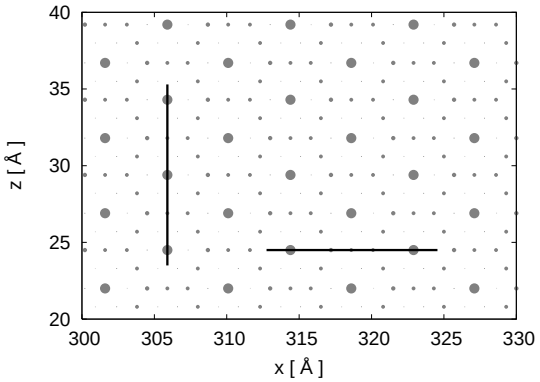

Fig. 5: Local energy cost for cleavage.

discrete, atomistic nature of matter can lead to differences in fracture behaviour, which cannot be explained by global continuum theories. The *microscopic* lattice trapping effect can strongly influence *macroscopic* properties like the crack velocity. To understand the reason for these observations, the simple picture shown in fig. 5 is sufficient. The radius of the given discs is proportional to the energy, which is needed for a local increase of the cleavage plane. In an oversimplified picture, this local energy cost shows, how much energy is needed to break "bonds" between the atoms. A vertical line represents a crack front moving in $[2\bar{1}\bar{1}]$ direction, a horizontal line a crack front propagating in $[0\bar{1}1]$ direction. From direct comparison, it is clear that the numbers of large discs per line length differ for the two cases, although the overall average over a larger area is the same. Thus, despite the fact that the two cracks see the same overall surface energy, the hard bonds that have to be broken instantaneously by a straight crack front differ. With this description it is understandable why the critical load for crack propagation varies for the two orientations. The initial barriers that have to be overcome are not the same.

Let us once more glimpse at the crack velocities for various loads and orientations. Fig. 6 shows the speed of cracks travelling on (010), (011) and (111) surfaces propagating in [101], [100], $[0\bar{1}1]$ and $[2\bar{1}\bar{1}]$ directions for k values between 1 and 1.8. Obviously, the velocity is increasing with increasing load. The cruxes indicate that only a selected part of the data has been included in the fit of v (before crack arrest or after initial acceleration, as shown in fig. 3 and fig. 4). All cracks need a certain overload for crack propagation, as $v = 0$ for $k = 1$. Obviously, the Griffith criterion only gives a lower bound for the energy needed for fracture and is thus not a sufficient criterion for fracture to occur. Once the crack starts moving, there is a lower limit for the steady state velocity. For high loads, the velocity seems to tend to an upper limiting threshold. The differences in the curves are attributed to a non-isotropic elastic behaviour of the cubic C15 phase as well as to the varying distribution of bonds, which is approached by the crack front (see above comparison on (111) fracture). The measured velocities range from about 0.4 $\frac{\text{km}}{\text{s}}$ to 1.5 $\frac{\text{km}}{\text{s}}$.

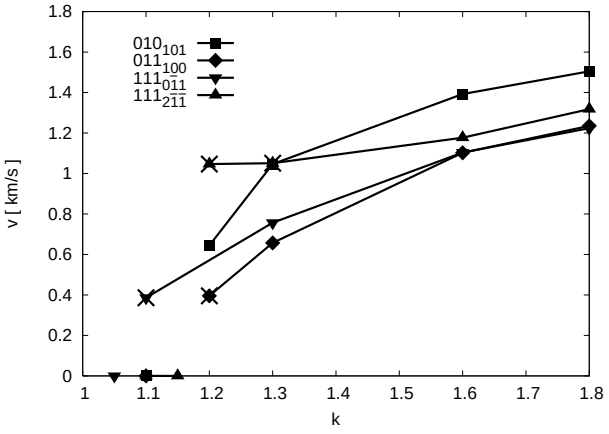

Fig. 6: Crack velocities.

The average transverse sound velocity [22] $\bar{v}_\mathrm{t}$ is about $2.7\frac{\mathrm{km}}{\mathrm{s}}$. Thus, the observed crack velocities are in a range of about 15-56% of $\bar{v}_\mathrm{t}$. A minimal non-zero value of the steady state crack velocity (a velocity gap) is well known from many molecular dynamics simulations. It can be interpreted as a consequence of rapidly snapping bonds [23]. When crack propagation becomes too slow, too much energy is dispersed from the crack tip by phonons before the crack arrives at the next bond. At a critical velocity, this bond will no longer break. A maximal crack velocity $v_\mathrm{max} = v_\mathrm{Rayleigh} \approx v_\mathrm{t}$ was proposed by Stroh [24], as a crack resembles a strong deformation of a free surface. The maximal observed velocity lies only slightly below the Yoffe value [25] $v_\mathrm{Y} \approx 0.6 v_\mathrm{t}$, which is related to the kinetic stability of a crack. Thus, the simulations yield an allowed velocity range for steady state crack propagation, which is triggered by the atomistic details of the samples.

How does the surface energy influence fracture? Following Griffith, planes of lowest surface energy should be the most likely cleavage planes. In fig. 7 (top) the surface energy is given for samples, which are cut on (010), (011) and (111) surfaces [26]. Obviously, all (010) and (011) planes possess the same surface energy, whereas two values are realized for the (111) planes. The Friauf-Laves phases can be interpreted as stackings of layers along the [111] direction (see *e.g.* [27,28]). The lowest surface energy is realized for cuts close to a kagome layer. Seed cracks on such layers were driven in fig. 2. The roughness at low loads is mainly limited by a motion of the crack above or below this kagome layer, as a deviation to other planes is suppressed by their increased surface energy. The surface energies obtained by flat cuts and by dynamic fracture for $k = 1.3$ are compared in fig. 7 (bottom). As a crack generates an upper and a lower fracture surface, these two values are indicated by triangles in the figure, whereas the average is given by circles. For all orientations the surfaces derived by fracture show higher average values than those for planar cuts. Thus, some of the surplus of energy due to the lattice-trapping effect causes roughness and an increased energy of the surfaces. For the near flat behavior

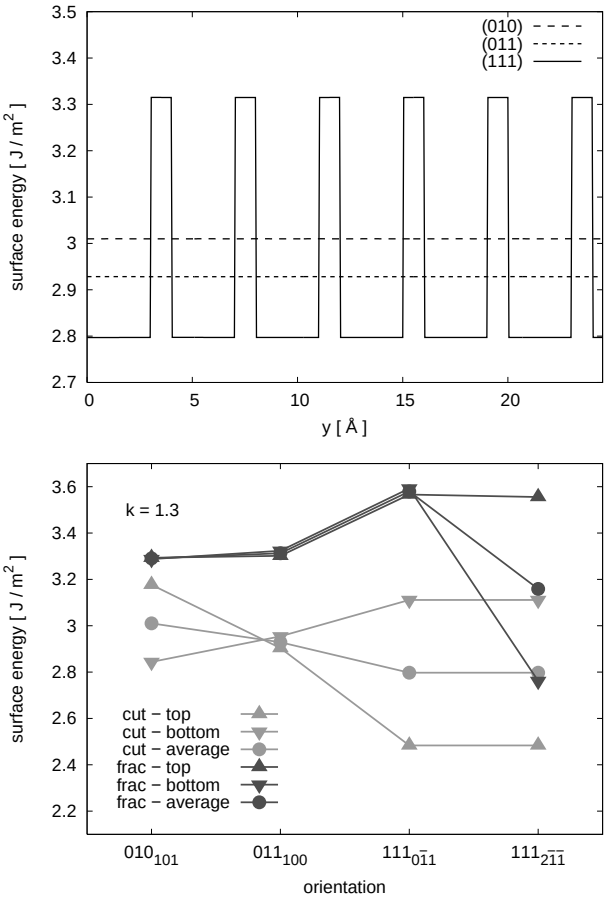

Fig. 7: Surface energies.

of the (111) crack propagating along the $[2\bar{1}\bar{1}]$ direction, the difference of the two fracture surfaces still shows up in unlike energies. However, for all the other orientations - where a distinct roughening on an atomic scale occurs - the surface energies of the two fracture surfaces are nearly identical (topmost curves). Thus, a crack tends to create upper and lower fracture surfaces, which need about the same energy to be created.

Conclusions

The discrete nature of matter is responsible for the lattice-trapping effect. It causes cracks to propagate only for loads above the Griffith criterion. As a consequence, the fracture surfaces are not implicitly those of lowest energy or lowest roughness. However, most of the surplus of energy causes radiation. The roughness and energy of the fracture surfaces as well as the path and speed of the cracks do not only depend on the cleavage plane but also on the in-plane crack propagation direction. This reveals the influence of the atomistic nature of matter. The number, strength and orientation of "bonds" approached by a crack define whether, where and how it propagates.

Acknowledgments

Support from the Deutsche Forschungsgemeinschaft under contract number TR 154/25-1 and within the Cluster of Excellence 310 (Simulation Technology) as well as by the European Network of Excellence on Complex Metallic Alloys (NMP3-CT-2005-500140) is gratefully acknowledged.

References

[1] A. A. Griffith, *Philos. Trans. R. Soc. Lond. Ser. A*, **221** (1921) 163.
[2] R. Thomson, C. Hsieh and V. Rana, *J. Appl. Phys.*, **42** (1971) 3154.
[3] F. Rösch, C. Rudhart, J. Roth, H.-R. Trebin and P. Gumbsch, *Phys. Rev. B*, **72** (2005) 014128.
[4] P. Gumbsch and R. M. Cannon, *Mat. Res. Soc. Bull.*, **25** (2000) 15.
[5] N. Bernstein and D. W. Hess, *Phys. Rev. Lett.*, **91** (2003) 025501.
[6] G. Csányi, T. Albaret, M. C. Payne and A. De Vita, *Phys. Rev. Lett.*, **93** (2004) 175503.
[7] T. Zhu, J. Li and S. Yip, *Phys. Rev. Lett.*, **93** (2004) 205504.
[8] M. J. Buehler, A. C. T. van Duin and W. A. Goddard III, *Phys. Rev. Lett.*, **96** (2006) 095505.
[9] A. Mattoni, M. Ippolito and L. Colombo, *Phys. Rev. B*, **76** (2007) 224103.
[10] J. H. Wernick, *Intermetallic Compounds*, edited by J. H. Westbrook (John Wiley & Sons, Incorporated) 1967, p. 197.
[11] IMD, the ITAP Molecular Dynamics Program http://www.itap.physik.uni-stuttgart.de/~imd
[12] M. S. Daw, S. M. Foiles and M. I. Baskes, *Mater. Sci. Rep.*, **9** (1993) 251.
[13] F. Ercolessi and J. B. Adams, *Europhys. Lett.*, **26** (1994) 583.
[14] VASP, the Vienna ab-initio simulation package http://cms.mpi.univie.ac.at/vasp/
[15] POTFIT - a force-matching program http://www.itap.physik.uni-stuttgart.de/∼imd/potfit/
[16] P. Brommer and F. Gähler, *Modelling Simul. Mater. Sci. Eng.*, **15** (2007) 295.
[17] F. Rösch, H.-R. Trebin and P. Gumbsch, *Int. J. Fracture*, **139** (2006) 517.
[18] F. Rösch, Doctoral thesis http://elib.uni–stuttgart.de/opus/volltexte/2008/3598/
[19] P. Gumbsch, S. J. Zhou and B. L. Holian, *Phys. Rev. B*, **55** (1997) 3445.
[20] S. J. Zhou, P. S. Lomdahl, R. Thomson and B. L. Holian, *Phys. Rev. Lett.*, **76** (1996) 2318.
[21] F. Rösch, H.-R. Trebin and P. Gumbsch, *Phil. Mag.*, **86** (2006) 1015.
[22] O. L. Anderson, *J. Phys. Chem. Solids*, **24** (1963) 909.
[23] M. Marder, *Comp. Sc. Eng.*, **1** (1999) 48.
[24] A. N. Stroh, *Advances in Physics*, **6** (1957) 418.
[25] E. H. Yoffe, *Phil. Mag.*, **42** (1951) 739.
[26] For a comparison of the derived surface energies to values obtained by ab-initio calculations, see [18], pp. 55-60 and references therein.
[27] P. M. Hazzledine and P. Pirouz, *Scr. Mat. Metall.*, **28** (1993) 1277.
[28] J. D. Livingston, *Phys. Stat. Sol. A*, **131** (1992) 415.